Amorphous and perovskite Li3xLa(2/3)-xTiO3 (thin) films via chemical solution deposition: solid electrolytes for all-solid-state Li-ion batteries

Peer-reviewed author version

VAN DEN HAM, Jonathan; PEYS, Nick; DE DOBBELAERE, Christopher; D'HAEN, Jan; Mattelaer, F.; Detavenier, C.; Notten, P. H. L.; HARDY, An & VAN BAEL, Marlies (2015) Amorphous and perovskite Li3xLa(2/3)-xTiO3 (thin) films via chemical solution deposition: solid electrolytes for all-solid-state Li-ion batteries. In: JOURNAL OF SOL-GEL SCIENCE AND TECHNOLOGY, 73 (3), p. 536-543.

DOI: 10.1007/s10971-014-3511-5
Handle: http://hdl.handle.net/1942/18555

Amorphous and perovskite Li_{3x} $La_{(2/3)-x}TiO_3$ (thin) films via chemical solution deposition: solid electrolytes for all-solid-state Li-ion batteries

E.J. van den Ham, N. Peys, C. De Dobbelaere, J. D'Haen , F. Mattelaer**, C. Detavernier**, P.H.L. Notten***, A.Hardy and M.K. Van Bael*
Hasselt University, Institute for Materials Research; Inorganic and Physical Chemistry and imec, division imomec, Martelarenlaan 42, B 3500 Hasselt, Belgium.
**Hasselt University, Institute for Materials Research; Material Physics and imec, division imomec, Martelarenlaan 42,B 3500 Hasselt, Belgium.*
***Ghent University, Department of Solid State Sciences, Krijgslaan 281, 9000 Ghent, Belgium.*
**** Energy Materials & Devices, Eindhoven University of Technology, 5600 MB Eindhoven, the Netherlands.*

corresponding author:
E.J. van den Ham
jonathan.vandenham@uhasselt.be
Tel: +32 11 26 83 93
Fax: +32 11 26 82 99

Keywords: Solid-electrolyte, thin films, aqueous CSD, Li-ion conductivity, half-cell

Abstract

Thin films of amorphous and crystalline perovskite Li_{3x} $La_{(2/3)-x}TiO_3$ (x=0.117) are prepared by means of aqueous chemical solution deposition onto rutile TiO_2 thin films as an anode, yielding an electrochemical half-cell. The Li-ion conductivity of the pin-hole free, amorphous LLT thin film (90 nm thick) is $3.8 \cdot 10^{-8}$ $S \cdot cm^{-1}$ on Pt and $1,3 \cdot 10^{-8}$ $S \cdot cm^{-1}$ on rutile TiO_2 , while measuring perpendicular to the thin film direction with impedance spectroscopy. Grazing angle attenuated total reflectance - Fourier transform infrared spectroscopy (GATR-FTIR) shows that all organic precursor molecules have been decomposed at 500°C. In addition, in-situ (heating) X-ray diffraction analysis shows that phase pure crystalline perovskite Li_{3x} $La_{(2/3)-x}TiO_3$ (x=0.117) is formed on top of the rutile TiO_2 anode at 700°C. Furthermore, thickness control is possible by varying the precursor solution concentration and the number of deposition cycles. The current study presents a promising synthesis route to develop all-solid-state battery devices based on multi-metal oxide materials using aqueous precursor chemistry.

E.J. van den Ham et al., Journal of Sol-Gel Science and Technology 73(3):536-543 DOI: 10.1007/s10971-014-3511-5

1. Introduction

In order to power autonomous electronic devices of tomorrow, such as wireless devices and body implants, efficient energy storage methods are required. Among other options, lithium-ion batteries (LIBs) in particular are interesting because of their high energy and high power density [1, 2]. Although widely applied, contemporary LIBs suffer from safety hazards and capacity fading [3]. Fabrication of all-solid-state batteries, where the liquid electrolyte is replaced with a solid electrolyte, is opted to circumvent these issues [4]. Recently, it was shown that excellent battery lifetimes can be established when a solid electrolyte is used [5]. In addition, solid electrolytes enable operation in a broader temperature range and exhibit a higher structural stability [3, 4]. Despite these advantages, most of solid electrolytes exhibit significantly lower Li-ion conductivity compared to their liquid counterparts. To ensure sufficient power density of the battery, ohmic loss over the electrolyte should be prevented. Since the charge transfer resistance follows the thickness of the electrolyte, thin films of solid electrolyte materials are required [1, 6].

Various solid electrolyte materials are available as bulk powder with a broad Li-ion conductivity range [7]. Based on its high Li-ion conductivity, perovskite $Li_{3x}La_{(2/3)-x}TiO_3$ (LLT) with x=0.117 is a promising solid electrolyte to be implemented in all-solid-state Li-ion batteries [8, 9]. In addition to the high conductivity of the perovskite phase (10^{-3} S/cm), the bulk material retains a high conductivity in the amorphous state (10^{-5} S/cm) [10, 11]. The main disadvantage of this electrolyte is its incompatibility with metallic lithium as an anode due to reduction of titanium (IV) around 1.5 V [9, 12] However, other anode materials with higher operating voltages are compatible with LLT. More specifically, LLT was synthesized in combination with $Li_4Ti_5O_{12}$ as an anode using macro porous morphologies to maximize the electrolyte-anode interface [10].

Several synthesis routes such as solid state synthesis [8] and sol-gel synthesis [13] yielding bulk LLT are known. In addition, several attempts have been made to combine anode or cathode materials with LLT, such as creating LLT coated $LiCoO_2$ particles [14] as well as preparing 3D ordered macro porous LLT to create an electrolyte network with high Li-ion conductivity surrounded by a $Li_4Ti_5O_{12}$ matrix [10]. However, only a limited number of studies focus on thin film synthesis of this material: pulsed laser deposition was applied several times to yield epitaxial LLT layers (approximately 40 nm thick) on $SrTiO_3$ and $NdGaO_3$ substrates [15],

E.J. van den Ham et al., Journal of Sol-Gel Science and Technology 73(3):536-543 DOI: 10.1007/s10971-014-3511-5

amorphous LLT films of approximately 500 nm were grown on quartz glass substrates [11] and both amorphous and crystalline LLT were deposited on Pt substrates with 400 nm thickness [16]. In addition, lanthanum deficient amorphous LLT ($Li_{0.32}La_{0.30}TiO_2$) was deposited on Si by atomic layer deposition, but crystallization yielded relatively rough morphologies combined with slow growth rates between 0,30 and 0.50 Å·cycle^{-1} [17]. A first attempt at preparing crystalline perovskite LLT films (x=0.167) on indium tin oxide using chemical solution deposition was carried out by Kitaoka et al [18]. Using three different organic precursors solutions based on metal alkoxides or acetates dissolved in 2-methoxyethanol, films with thicknesses ranging from 200 nm to 1 µm were obtained by dip coating in combination with a post-deposition anneal of 700 to 1300°C [18].

In the current study, amorphous and crystalline perovskite LLT thin films were prepared directly on a rutile TiO_2 anode film (with Pt underneath) or on a blank Pt current collector by chemical solution deposition using an aqueous precursor solution containing Li^+, La^{3+} and Ti^{4+}. While the latter stack allows determination of the material's Li-ion conductivity, the former allows studying the interfacial reactions between a suitable anode material (rutile TiO_2) and the electrolyte under study, which is important with respect to the material's final application in a functioning battery device.

2. Experimental

2.1 Precursor synthesis

Aqueous precursor solutions were prepared for Li^+, La^{3+} and Ti^{4+}. Lithium nitrate ($LiNO_3$, Sigma Aldrich, ≥98.5%) and lanthanum nitrate hexahydrate ($Li(NO_3)_3·6H_2O$, Sigma Aldrich, ≥99%) were both dissolved in water by stirring at room temperature, yielding concentrations of 1.5 mol·L^{-1} and 1.0 mol·L^{-1} respectively. Titanium isopropoxide ($Ti[OCH(CH_3)_2]_4$, Sigma Aldrich, ≥97%) was added to water to form titanium hydroxide, followed by addition of citric acid (CA, Sigma Aldrich, ≥99%), hydrogen peroxide (H_2O_2, Acros Organics, 35%) and ammonia (NH_3, Merck, 32%) to yield a citrate-peroxo-Ti(IV) solution with a 0.9 mol·L^{-1}. A detailed description of the citrate-peroxo-Ti(IV) precursor was reported earlier by Hardy et al. [19].

The concentrations of the mono-ion solutions was determined by inductively coupled plasma-atomic emission spectroscopy (ICP-AES, Optima 3300, PerkinElmer) before mixing them together in stoichiometric amounts at room temperature (Fig. 1). The final multi-metal ion precursor solution was prepared in a high (0.95

E.J. van den Ham et al., Journal of Sol-Gel Science and Technology 73(3):536-543 DOI: 10.1007/s10971-014-3511-5

M) and low (0.38 M) total metal ion concentration with a Li^{+}:La^{3+}:Ti^{4+} molar ratio of 0.35:0.55:1.00 (i.e. x=0.117).

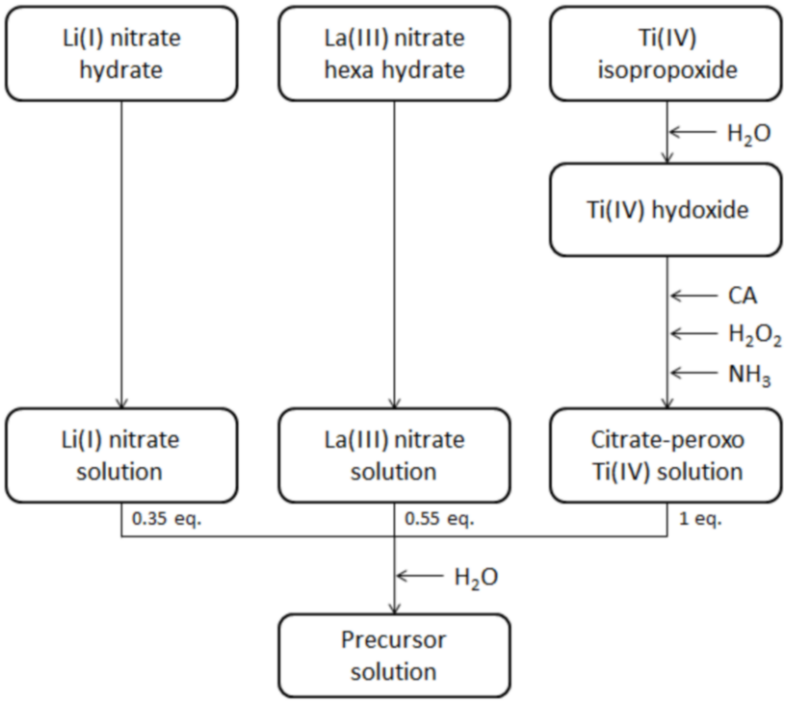

Figure 1: Synthesis scheme of the aqueous precursor solution.

2.2 Thin film deposition

The aqueous multi-metal ion precursor solution was spin-coated (3000 rpm, 30 s, 1000 rpm/s) onto small pieces (3 x 3 cm) of different substrates, designated as follows: TiO_2 (Si); a stack of TiO_2/Si (p-type Si with 90 nm TiO_2 [20]), TiO_2 (Pt); a stack of TiO_2/Pt/TiN/Si (40 nm TiN coated p-type Si with 70 nm Pt with 90 nm TiO_2, deposited as mentioned in [20]) and Pt; a stack of Pt/TiN/Si (40 nm TiN coated p-type Si with 70 nm Pt).

All these substrates were cleaned by an UV/O_3 treatment at 60 °C (40 min., Novascan PSD Pro Series). Hot plate treatments were carried out in ambient air after spin coating of the aqueous precursor at 250 °C (2 min.), 375 °C (2 min.) and 500 °C (2 min.). The sequence of spin coating and hot plate treatment was repeated multiple times to obtain films with the desired thickness. The final film was annealed by either a heat treatment at 500 °C (1 to 4 hours) in static air on a hot plate or at 700 °C (1 to 4 hours) under a dynamic air flow (0.1 L·min^{-1}) in a tube furnace.

2.3 Powder characterization

E.J. van den Ham et al., Journal of Sol-Gel Science and Technology 73(3):536-543 DOI: 10.1007/s10971-014-3511-5

The thermal decomposition profile of the yellow precursor powder, obtained by drying the precursor solution at 60°C, was investigated by thermogravimetric analysis with coupled differential scanning calorimetry (TGA/DSC, TA instruments SDT Q600). 6 mg of the powder was heated ramped at 10°C/min up to 1200°C using dry air (0.1 $L \cdot min^{-1}$) in an alumina crucible. The crystallization process of the aqueous precursor powder was studied by High-Temperature X-Ray Diffraction analysis (HT-XRD, Bruker D8 with an Anton Paar HTK1200 high temperature chamber with a kapton window) from 250 - 900°C ($10°C \cdot min^{-1}$), in steps of 50°C with a counting time of 52.8 s per step. The yellow precursor powder was submitted to a pre-anneal (250°C in a drying oven overnight) to remove most of the organics before starting the HT-XRD experiment.

2.4 Thin film characterization

As-deposited and sequentially heated (250, 375, 500 and 700°C) layers were characterized by grazing angle attenuated total reflectance - Fourier transform infrared spectroscopy separately (GATR-FTIR, Bruker Vertex 70 combined with Harrick 65° single reflection Ge-ATR) from 4000 to 600 cm^{-1} with 32 scans per sample with a torque of 24 kPa. Crystallization of amorphous LLT thin films was studied by in-situ heating XRD (Bruker D8 Discover with experimental heating chamber [21]). A linear detector was used, recording a diffraction pattern with a 2θ range of 30 to 50° every 5 seconds within a temperature range of 25 to 900°C (with a heating rate of $1°C \cdot min^{-1}$). The morphology of annealed LLT films was investigated by means of scanning electron microscopy (SEM, FEI Quanta 200F). Finally, the Li-ion conductivity of LLT thin films was studied by means of Impedance Spectroscopy. Hereto, Au electrodes (300 nm thick, 6 mm^2 area) were evaporated (Vactec thermal evaporator, $3 \cdot 10^{-7}$ mbar) on top of post-annealed LLT thin films with Pt or TiO_2 (Pt) as the underlying substrate. The Li-ion conductivity perpendicular to the film direction is of importance for the power density of the final battery, therefore the electric field was applied in this direction. The impedance was measured using an Autolab PGSTAT302N with frequencies ranging from 1MHz – 10 mHz with an alternating voltage of 3 mV. The results were fitted with equivalent circuit models with resistor (R) and capacitor (C) elements using Nova software (Version 1.9.16, Metrohm Autolab B.V.).

3. Results and discussion

E.J. van den Ham et al., Journal of Sol-Gel Science and Technology 73(3):536-543 DOI: 10.1007/s10971-014-3511-5

Powders

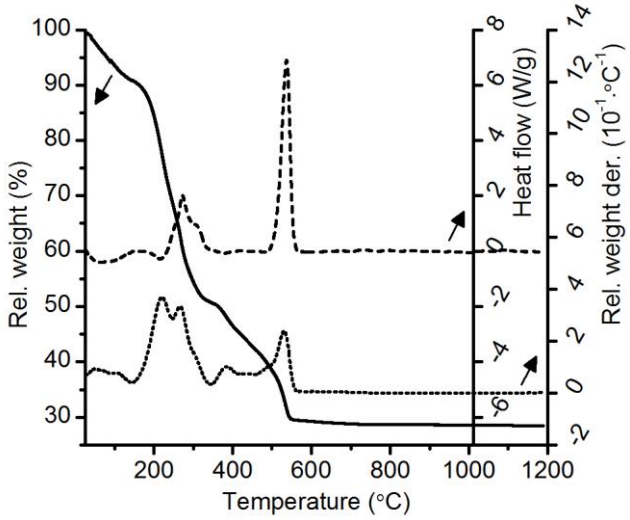

Figure 2: TGA/DSC graph of dried (60°C overnight) LLT precursor gel, showing the relative weight (solid line), heat flow (dashed line) and relative weight derivative (dotted line) as a function of temperature (10°C·min^{-1}, with dry air flow of 0.1 L·min^{-1}). The arrows indicate the signal specific Y-axis.

E.J. van den Ham et al., Journal of Sol-Gel Science and Technology 73(3):536-543 DOI: 10.1007/s10971-014-3511-5

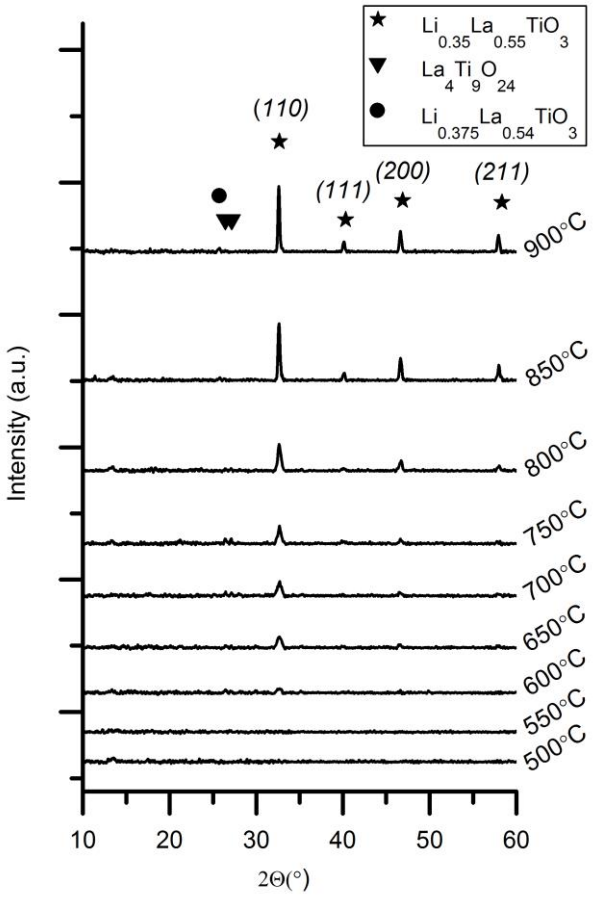

Figure 3: HT-XRD patterns a of dried and pre-calcined (250°C) precursor powder measured at several temperatures with a heating rate of 10°C·min^{-1} in dry air (0.1 L·min^{-1}). Reference patterns of LLT (stars, x=0.117, JCPDS 46-0465) are shown, along with the most intense peaks of $La_4Ti_9O_{24}$ (triangles, JCPDS 036-0137) and $Li_{0.375}La_{0.54}TiO_3$ (circles, JCPDS 47-0668).

The thermal decomposition pathway of the dried aqueous precursor gel (Fig. 2, solid line) shows a weight loss between room temperature and 150 °C, which is most likely the loss of water. Above 150 °C, a major weight loss is observed while the heat flow (Fig. 2, dashed line) indicates that this is accompanied with small endothermic step at 220°C followed by a sequence of exothermic events at 270 and 535°C, respectively. This sequence is possibly related to the decomposition of organics and nitrates. Above 600 °C, no significant weight loss is observed, indicating that the precursor has completely decomposed, and most probably only oxide phase(s) remain. HT-XRD analysis (Fig. 3) indeed indicates that the onset of perovskite LLT crystallization (JCPDS 46-0465) occurs at 600°C. From 600 to 850 °C small peaks are present around 26,4 and 27,2° 2θ, suggesting the presence of $La_4Ti_9O_{24}$ (JCPDS 036-0137) as a secondary phase. These small peaks disappear at 900°C, but at this temperature a small single peak at 25,7° 2θ can be observed, suggesting that $La_4Ti_9O_{24}$ transformed into

E.J. van den Ham et al., Journal of Sol-Gel Science and Technology 73(3):536-543 DOI: 10.1007/s10971-014-3511-5

$Li_{0.375}La_{0.54}TiO_3$ (JCPDS 47-0668) at higher temperatures, possibly by reacting with a lithium containing amorphous phase.

Thin films

After showing the suitability of the water based precursor system to obtain LLT powders, the behavior of thin films formation was studied. Due to differences in the surface to volume ratio between powders and thin films, leading to different heat transport and gas diffusion phenomena, their decomposition process may differ [22]. Therefore, the decomposition process was indirectly studied on the thin films, by identification of the organic residuals using GATR-FTIR.

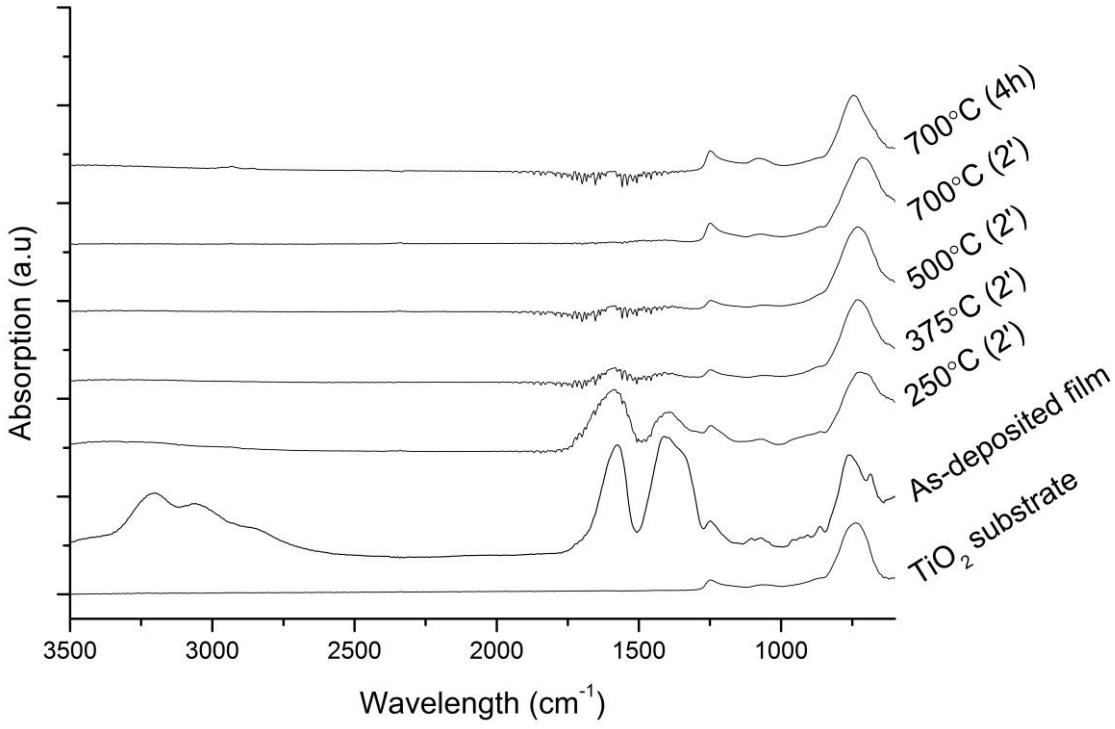

Figure 4: GATR-FTIR of the blank TiO_2(Si) substrate, the as-deposited aqueous precursor and different heat treated LLT layers on TiO_2 (Si). The spectra were recorded directly after spin coating (as-deposited) or after consecutive hotplate steps for 2 minutes at 250°C, 250°C+375°C or 250°C+375°C+500°C under static air. Samples annealed at 700°C (for 2 minutes or for 4 hours) were placed in a pre-heated tube furnace in dry air after completing all consecutive hotplate steps.

E.J. van den Ham et al., Journal of Sol-Gel Science and Technology 73(3):536-543 DOI: 10.1007/s10971-014-3511-5

GATR-FTIR was applied on a single layer deposited onto the TiO_2 (Si) substrate; measured as-deposited and directly after different heat treatments (Fig. 4). The TiO_2 (Si) substrate shows a strong band at 750 cm^{-1}, arising from TiO_2 lattice vibrations [23, 24]. Si-O-Si longitudal and transverse modes are also observed at 1250 and 1050 cm^{-1}, respectively [25]. For the as-deposited aqueous precursor several bands could be observed: the (broad) band at 3500 to 2750 cm^{-1} is associated with C–H stretching vibrations, O-H stretching vibrations of (unbound) water and NH_4^+ anti-symmetric stretching vibrations broadened by hydrogen bond formation [26, 27]. At 1600 and 1400 cm^{-1} strong bands are observed, associated with COO^- asymmetric and symmetric stretching vibrations of the citrate ligands [27]. In addition, the 1400 cm^{-1} band overlaps with the asymmetric stretching vibration of NO_3^- [28]. The (weak) band at 1250 cm^{-1} is assigned to C-OH stretching of a carboxylic acid, related to citric acid [27]. Finally, the (weak) bands at 850 to 800 cm^{-1} and 770 to 715 cm^{-1} are both related NO_3^-, respectively out-of-plane and in-plane bending vibrations [26, 28].

At 250°C the broad band from 3500 to 2750 cm^{-1} is strongly reduced, associated with the removal of water and NH_4^+. Furthermore, a large reduction of the 1400 cm^{-1} band combined with absence of the weak bands at 850-800 cm^{-1} and 770-715 cm^{-1} suggest that NO_3^- has been removed from the sample. At 375°C, the 1600 and 1400 cm^{-1} band have strongly been reduced, indicating that most of the organic materials have been decomposed. At 500°C and above only bands related to substrate can clearly be observed. Furthermore, above 375°C no bands are observed between 1550-1300 cm^{-1}, indicating that no (oxy)carbonates [23, 26, 29] are formed. In literature no FTIR results could be found regarding (perovskite) LLT. However, bands of closely related titanates are only visible at lower wavenumbers than recorded in this study [26, 30]. In-situ XRD was therefore employed to study the crystallization of the films obtained with little organic residuals prepared at 500°C.

E.J. van den Ham et al., Journal of Sol-Gel Science and Technology 73(3):536-543 DOI: 10.1007/s10971-014-3511-5

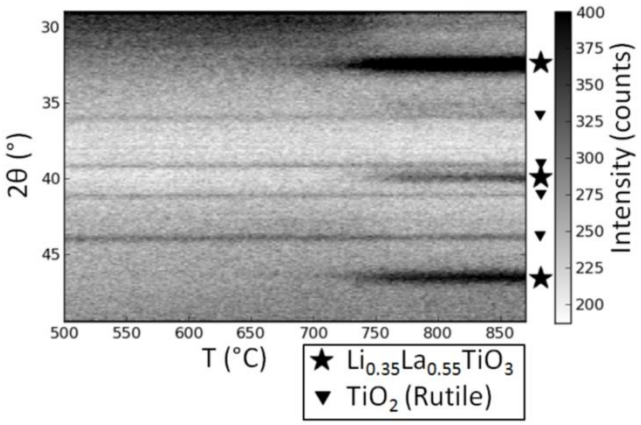

Figure 5: XRD intensity of a 240 nm thick LLT film on TiO_2 (Si), pre-annealed at 500° for 1 hour in static air, as a function of temperature during non-isothermal heating with a heating rate of 6°C·min^{-1} in static air. Reference peak positions of perovskite LLT (stars, x=0.117, JCPDS 046-0465) and rutile TiO_2 (triangles, JCPDS 021-1276)

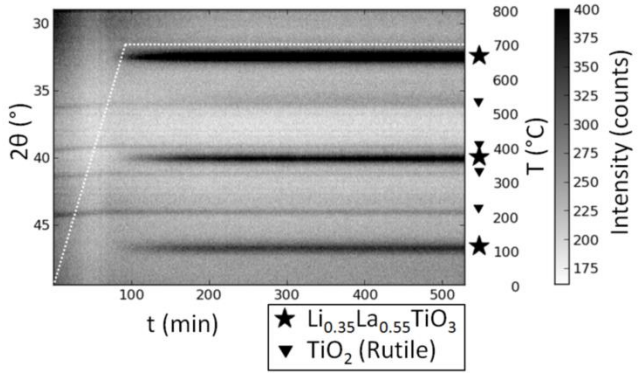

Figure 6: XRD intensity of a 240 nm thick LLT film on TiO_2 (Si), pre-annealed at 500° for 1 hour in static air, heated isothermally at 700°C with in static air (after a short period of non-isothermal heating to reach 700°C with 10°C·min^{-1}). The temperature profile is plotted (dashed line) as a function of time. Reference peak positions of perovskite LLT (stars, x=0.117, JCPDS 046-0465) and rutile TiO_2 (triangles, JCPDS 021-1276)

The crystallization process of LLT thin films, deposited on TiO_2 (Si) and pre-annealed at 500°C, was examined by in situ X-ray diffractometry as a function of temperature during its non-isothermal heating with constant heating rate (Fig. 5) and as function of time during isothermal heating at 700°C (Fig. 6). Before the heating starts, diffractions are only visible at 2θ = 36, 39, 41 and 44°; all these correspond to the rutile phase (JCPDS 021-1276) of the TiO_2 anode underneath the amorphous LLT film. While heating the amorphous LLT films, the onset of perovskite LLT (x=0.117, JCPDS 046-0465) crystallization can be observed at 725°C, identified

E.J. van den Ham et al., Journal of Sol-Gel Science and Technology 73(3):536-543 DOI: 10.1007/s10971-014-3511-5

by the 33, 40 and 47° 2θ angle diffractions. Isothermal heating at a slightly lower temperature of 700°C leads to perovskite LLT phase formation as well (Fig. 6), but prolonged heating at this temperature is required to fully crystallize the film.

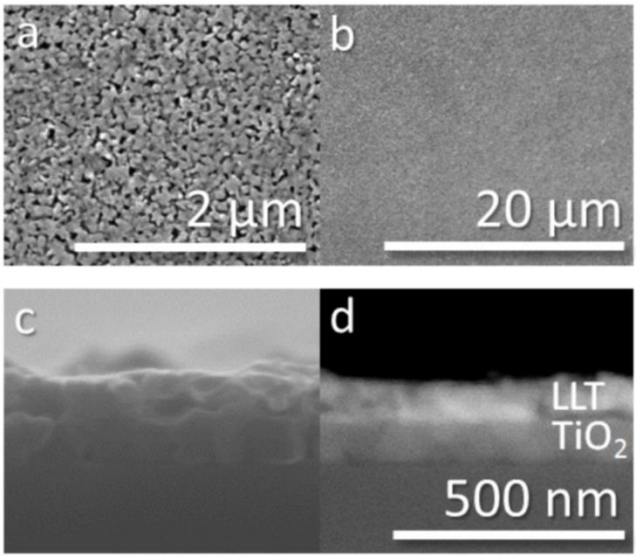

Figure 7: Top view SE images at different magnifications (a & b) and cross sections SE image (c) and BSE image (d) and of 4 layers (0.38 M) of LLT deposited on TiO_2 (Si) annealed at 700°C for 1 hour in dry air.

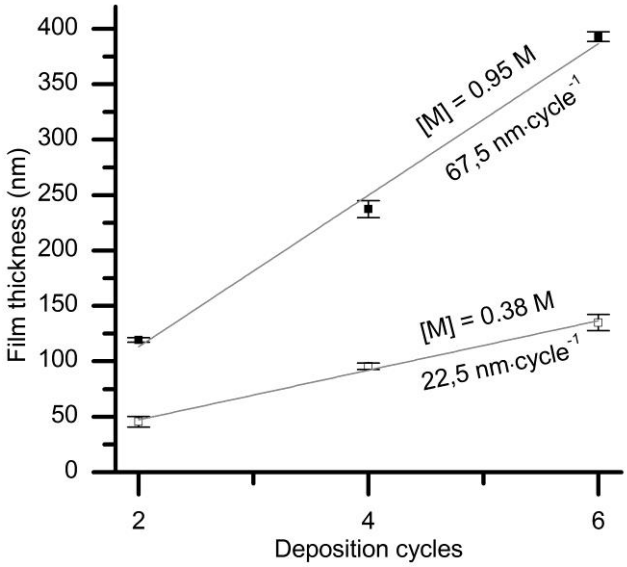

Figure 8: LLT film thickness as function of deposition cycles and precursor concentration deposited on TiO_2 (Si), determined by SEM cross sections. After deposition the LLT films were annealed for 1 hour at 700°C in dry air. High (0.95M; black squares) and low concentrations (0.38 M; white squares) were measured with the standard deviation shown for each sample.

E.J. van den Ham et al., Journal of Sol-Gel Science and Technology 73(3):536-543 DOI: 10.1007/s10971-014-3511-5

The top view SEM micrographs show crystalline perovskite LLT films on TiO_2 (Si) (Fig. 7a and 7b), which received an anneal comparable to the isothermal heating during the in-situ XRD study (Fig. 6). The films exhibit a homogeneous morphology with macro porosity. It is speculated (based on properties of the amorphous layers, see further in Fig. 9) that this is introduced during the crystallization of the films. Using the Z contrast in the BSE cross section image (Fig. 7d) the LLT layer (brighter, 90 nm thick) can clearly be distinguished from the rutile TiO_2 anode layer (darker, 90 nm thick) underneath. The thickness of the LLT layer on TiO_2 increases linearly with the number of deposition cycles for high and low precursor solution concentrations (Fig. 8).

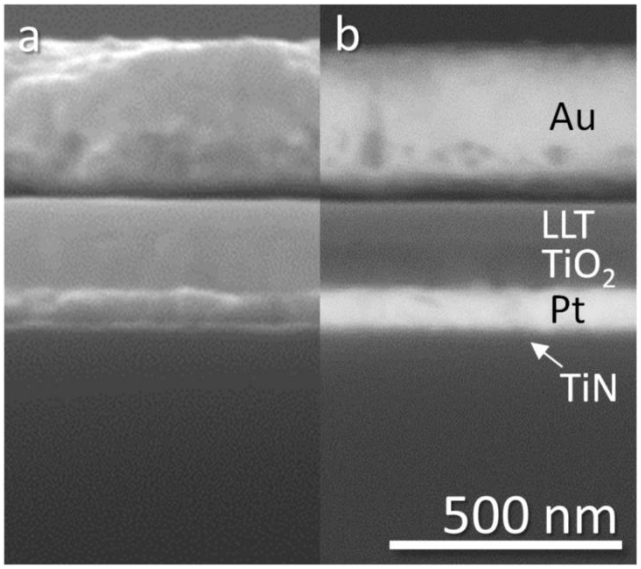

Figure 9: Cross section SEM SE (a) and BSE (b) images of 4 layers (0.38 M) of amorphous LLT deposited on TiO_2 (Pt) annealed at 500°C for 4 hours in static air. Afterwards, the Au electrode was evaporated on top.

E.J. van den Ham et al., Journal of Sol-Gel Science and Technology 73(3):536-543 DOI: 10.1007/s10971-014-3511-5

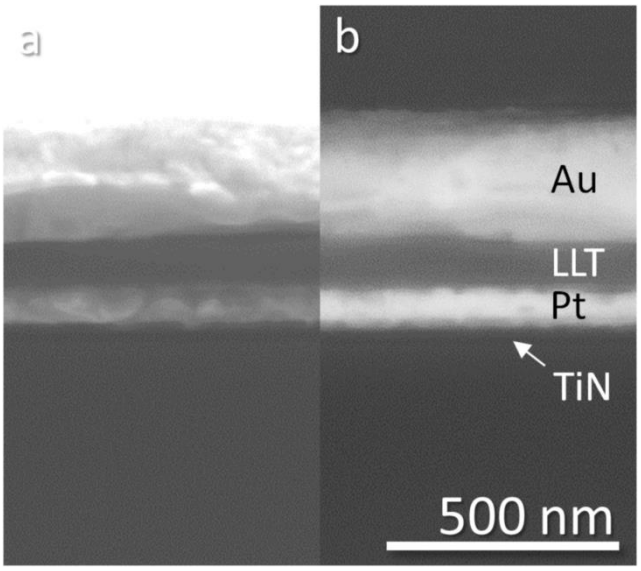

Figure 10: Cross section SEM SE (a) and BSE (b) images of 4 layers (0.38 M) of amorphous LLT deposited on Pt, annealed at 500°C for 4 hours in static air. Afterwards, the Au electrode was evaporated on top.

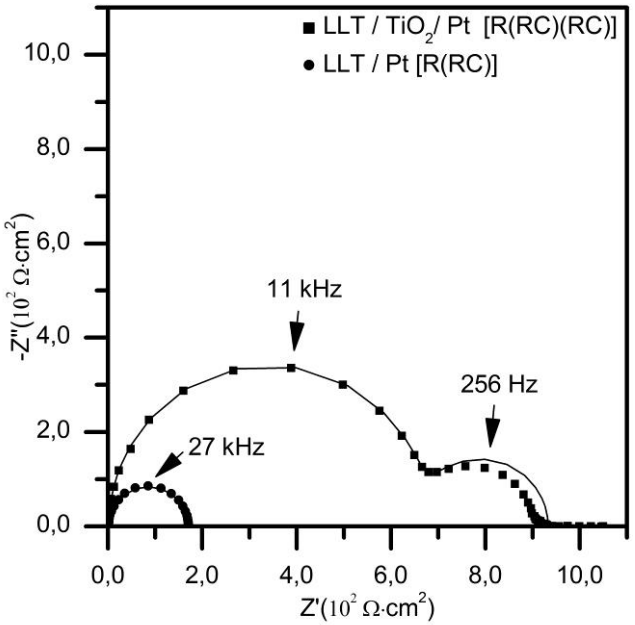

Figure 11: Nyquist plot of 90 nm thick LLT films annealed for 4 hours at 500°C, with 300 nm Au electrodes evaporated on top. Two semi-circles are observed for LLT on TiO_2 (Pt) (squares) as shown in Fig. 9, wheras one semi-circle was observed for LLT on Pt (circles) as shown in Fig. 10. Results of the fitted equivalent circuit models are also shown (grey lines) with resistor (R) and capacitor (C) elements.

Thus far, XRD and GATR-FTIR results have, respectively, confirmed the formation of perovskite phase LLT on TiO_2 (Si) and the presence of negligible organic contents in the films. To study functional properties of these

E.J. van den Ham et al., Journal of Sol-Gel Science and Technology 73(3):536-543 DOI: 10.1007/s10971-014-3511-5

films with impedance spectroscopy, an electronically conductive substrate is required; for this study Pt coated substrates are used. To ensure stability of the current collector and limit the macro porosity of the films, the maximum annealing temperature was set at 500°C, yielding smooth amorphous LLT thin films (Fig. 9 and 10). The impedance results (Fig. 11) show one semicircle for LLT on Pt, and two semicircles in case of the half-cell configuration (LLT on TiO_2(Pt)). Based on this comparison, it is assumed that the high frequency range semi-circle is related to the amorphous LLT layer, whereas the small low-frequency range semi-circle is related to TiO_2 layer. The later can either arise from Li^+ ions that have diffused from the LLT layer into TiO_2 during annealing (4 hours at 500°C), or it can be related to the charge transfer resistance at the LLT-TiO_2 interface. Based on fitting with an equivalent circuit, the Li-ion conductivities of amorphous LLT thin films, with thicknesses under 100 nm, on Pt and TiO_2 (Pt) were found to be $3{,}8 \cdot 10^{-8}$ $S \cdot cm^{-1}$ and $1{,}3 \cdot 10^{-8}$ $S \cdot cm^{-1}$, respectively. Since the conductivity of amorphous LLT films drops when the lithium contents is reduced [11], the lower conductivity of the LLT thin film on TiO_2 (Si) might arise from a lithium deficiency. The conductivities obtained with the current approach are considerably lower compared to the conductivity of bulk amorphous LLT prepared at 600°C (10^{-5} S/cm, measured at room temperature) [10]. Although a previous study on LLT thin films (with a thickness under 100 nm) prepared at higher temperatures nearly accomplished this value, the reported Li-ion conductivity was measured in lateral direction [15], whereas the current study regards the perpendicular Li-ion conductivity of the thin film, which is of higher relevance for the final battery.

Conclusion

The results of the current study have shown that amorphous and crystalline perovskite LLT (thin) films could be established using an aqueous precursor system, at respectively 500 and 700°C. The thickness of the films can easily be tuned by varying the number of deposition cycles and the concentration of the aqueous precursor, which is of importance to tailor the ideal electrolyte thickness in a battery device. In addition, the uniform depositions on the rutile TiO_2 anode and Pt current collector indicate that the current approach has potential to be applied to other anode and cathode materials as well. The impedance results of the amorphous LLT thin films showed that an electronic short circuit could be prevented across the films, indicating that no pin holes are present and that the amount of residual organics is sufficiently low at 500°C. The final value obtained for the Li-ion conductivity of the amorphous thin films (10^{-8} $S \cdot cm^{-1}$) still has to be improved in view the

E.J. van den Ham et al., Journal of Sol-Gel Science and Technology 73(3):536-543 DOI: 10.1007/s10971-014-3511-5

application of LLT as a solid electrolyte. Nevertheless, it is a promising result compared to other studies on LLT thin films.

Acknowledgements

The authors acknowledge financial support by the IWT Flanders (SBO project SOSLion). Christopher De Dobbelaere is a Post-Doctoral Research Fellow of the Research Foundation Flanders (FWO-Vlaanderen). Tim Vangerven and Peter-Paul Harks are acknowledged for preparing and starting up the impedance spectroscopy measurements. Thanks to Elsy Thijssen for performing the ICP-AES measurements and Hanne Damm for the thermal analysis. Special thanks to Bart Ruttens for all the work regarding SEM and XRD samples.

References

[1] J.F.M. Oudenhoven, L. Baggetto, P.H.L. Notten, “All-Solid-State Lithium-Ion Microbatteries: A Review of Various Three-Demenisional Concepts”, Adv. Energy Mater., vol. 2011, no. 1, pp. 10-33, 2011.

[2] J.W. Long, B. Dunn, D.R. Rolison, H.S. White, “Three-Dimensional Battery Architectures”, Chem. Rev., vol. 104, no. 10, pp. 4463-4492, 2004.

[3] V. Thangadurai, W. Weppner, “Recent progress in solid oxide and lithium ion conducting electrolytes research”, Ionics, vol. 12, pp. 81-92, 2006.

[4] P. Knauth, “Inorganic solid Li ion conductors: An overview”, Sol. State Ion., pp. 911-916, 2009.

[5] L. Bagetto, R.A.H. Niessen, P.H.L. Notten, “High energy density all-solid-state batteries: a challenging concept towards 3D integration”, Adv. Funct. Mater., vol. 18, pp. 1057-1066, 2008.

[6] M. Roberts, P. Johns, J. Owen, D. Brandell, K. Edstrom, G.E. Enany, C. Guery, D. Golodnitsky, M. Lacey, C. Lecoeur, H. Mazor, E. Peled, E. Perre, M.M. Shaijumon, P. Simon, P.L. Taberna, “3D lithium ion batteries—from fundamentals to fabrication”, J. Mater. Chem., vol. 21, pp. 9876-9890, 2011.

[7] K. Takada, “Progress and prospective of solid-state lithium batteries”, Acta Materialia, vol. 61, pp. 759-770, 2013.

[8] Y. Inaguma, C. Liquan, M. Itoh, T. Nakamura, “High ionic conductivity in lithium lanthanum titanate”, Sol. State Commun., vol. 861, no. 10, pp. 689-693, 1993.

[9] S. Stramare, V. Thangadurai, W. Weppner, “Lithium Lanthanum Tinanates: a review”, Chem. Rev., vol. 15, no. 21, pp. 3974-3990, 2003.

[10] K. Kanamura, N. Akutagawa, K. Dokko, “Three dimensionally ordered composite solid materials for all solid/state rechargeable lithium batteries”, J. Power Sources, pp. 86-89, 2005.

[11] S. Furusawa, H. Tabuchi, T. Sugiyama, S. Tao, J.T.S. Irvine, “Ionic conductivity of amorphous lithium lanthanum titanate thin film”, Sol. State Ion., vol. 176, pp. 553-558, 2005.

[12] Y.J. Shan, L. Chen, Y. Inaguma, M. Itoh, T. Nakamura, “Oxide cathode perovskite structure for rechargeable lithium batteries”, J. Power Sources, vol. 54, pp. 397-402, 1995.

[13] H. Geng, J. Lan, A. Mei, Y. Lin, C.W. Nan, “Effect of sintering temperature on microstructure and transport properties of Li3xLa2/3−xTiO3 with different lithium contents”, Electrochimica Acta, pp. 3406-4314, 2011.
[14] S. Noh, J. Kim, M. Eom, D. Shin, “Surface modification of LiCoO2 with Li3xLa2/3−xTiO3 for all-solid-state lithium ion batteries using Li2S–P2S5 glass–ceramic”, Ceram. Int., vol. 39, no. 7, p. 8453–8458, 2013.
[15] T. Ohnishi, K. Takada, “Synthesis and oriented control of Li-ion conducting epitaxial Li0.33La0.56TiO3 solid electrolyte thin films by pulsed laser deposition”, Sol. State Ion., pp. 80-82, 2012.
[16] J.K. Ahn, S.G. Yoon, “Characteristics of perovskite (Li0.5La0.5)TiO3 solid electrolyte thin films grown by pulsed laser deposition for rechargeable lithium microbattery”, Electrochimica Acta , vol. 50, pp. 371-374, 2004.
[17] T. Aaltonen, M. Alnes, O. Nilsen, L. Costelle, H. Fjellvag, “Lanthanum titanate and lithium lanthanum titanate thin films grown by atomic layer deposition”, J. Mater. Chem., vol. 20, pp. 2877-2881, 2010.
[18] K. Kitaoka, H. Kozuka, T. Hashimoto, T. Yoko, “Preparation of La0.5Li0.5TiO3 perovskite thin films by sol-gel method”, J. Mater. Sci., pp. 2063-2070, 1997.
[19] A. Hardy, J. D'Haen, M.K. Van Bael, J. Mullens, “An aqueous solution–gel citratoperoxo–Ti(IV) precursor:synthesis, gelation, thermo-oxidative decomposition and oxide crystallization”, J. Sol-Gel Sci. Technol., vol. 44, pp. 65-74, 2007.
[20] I. Truijen, M.K. Van Bael, H. van den Rul, J. Mullens, “Synthesis of thin dense titania films via an aqueous solution-gel method”, J. Sol-Gel Sci. Technol., pp. 43-48, 2007.
[21] W. Knaepen, C. Detavenier, R.L. van Meirhaege, J. Jordan Sweet, C. Lavoie, “In-situ X-ray Diffraction study of Metal Induced Crystallization of amorphous silicon”, Thin Sol. Films, vol. 516, no. 15, pp. 4946-4952, 2008.
[22] D. Sanchez-Rodriguez, J. Farjas, P. Roura, S. Richart, N. Mestres, X. Obradors, T. Puig, “Thermal Analysis for Low Temperature Synthesis of Oxide Thin Films from Chemical Solutions,” J. Phys. Chem. C, vol. 117, pp. 20133-20138, 2013.
[23] P.A. Connor, K. D. Dobson, A. J. McQuillan, “Infrared Spectroscopy of the TiO2 / Aqueous Solution Interface,” Langmuir, vol. 15, pp. 2402-2408, 1999.
[24] V.C. Farmer, The Infrared Spectra of Minerals, 1974.
[25] D. Rouchin, N. Rochat, F. Gustavo, A. Chabli, O. Renault, P. Besson, “Study of ultrathin silicon oxide films by FTIR-ATR and ARXPS after wet chemical cleaning processes,” Surf. Interface Anal., vol. 34, pp. 445-450, 2002.
[26] R.A. Nyquist, C.L. Putzig, M.A. Leugers, Handbook of Infrared and Raman Spectra of Inorganic Compounds and Organic Salts, Massachudetts: Academic Press, 1997.
[27] A. Hardy, D. Nelis, G. Vanhoyland, M.K. Van Bael, H. Van den Rul, J. Mullens, L.C. Van Poucke, J. D’Haen, L. Goux, D.J. Wouters, “Effect of pyrolysis temperature on the properties of Bi3.5La0.5Ti3O12 thin films deposited by aqueous chemical solution deposition,” Mater. Chem. Phys., vol. 92, no. 2-3, pp. 431-437, 2005.
[28] Q. Zhang, Y.Zhang, C. Cai, Y. Guo, J.P. Reid,Y. Zhang, “In Situ Observation on the Dynamic Process of Evaporation and Crystallization of Sodium Nitrate Droplets on a ZnSe Substrate by FTIR-ATR,” J. Phys. Chem. A, vol. 118, pp. 2728-2737, 2014.
[29] S. Irusta, L.M. Cornaglia, E.A. Lombardo, “Effects of rhodium and platinum on the reactivity of lanthanum phases,” Mater. Chem. and Phys., vol. 86, pp. 440-447, 2004.
[30] R. Salzer, J. Dressler, M.K. Gergs, D. Michel, H. Schlemmbach, W. Windsch, P. Reich, “Structural investigation of (Pb,La)TiO3 ceramics by second derivative FTIR spectroscopy,” J. Mol. Struct., vol. 219, pp. 177-182, 1990.